Fast Growth and Broad Applications of 25-Inch Uniform Graphene Glass

Xu-Dong Chen, Zhaolong Chen, Wen-Shuai Jiang, Cuihong Zhang, Jingyu Sun, Huihui Wang, Wei Xin, Li Lin, Manish K. Priydarshi, Huai Yang, Zhi-Bo Liu, Jian-Guo Tian, Yingying Zhang, Yanfeng Zhang,* and Zhongfan Liu**

Graphene, the first 2D atomic-crystalline material available to us, possesses a number of superior properties,[1–6] making it suitable for use in photocatalysis,[7] transparent electrodes,[8] supercapacitors,[9] and photodetectors.[10,11] To fulfill the growing demand for graphene, various synthetic methods have been developed by far.[1,2,12–19] In particular, the chemical vapor deposition (CVD) growth of graphene on metal substrates has presented unique advantages in terms of the scalable production of uniform graphene samples with a large domain size and a tunable film thickness.[16–19] However, such a route involves transferring as-synthesized graphene onto target (insulating) substrates, which is a complicated and tedious process and often results in the introduction of defects and contaminants into the samples. This often gives rise to significant degradation in the graphene quality and hence device performance.[8,20–22] Consequently, methods that allow direct deposition of graphene on insulating substrates are highly desirable.

Till date, direct growth of graphene has been realized on a variety of dielectric and insulating substrates, such as SiO_2,[23,24] Si_3N_4,[25] sapphire,[26] and boron nitride (BN).[27,28] However, the carrier mobilities in such directly grown graphene samples[23,24] are not significantly higher than those in the transferred graphene samples.[8,22,29] In order to increase the practical usability of graphene, composites consisting of daily use materials and graphene are being explored extensively. Our group reported the direct growth of graphene on glass, a typical transparent and insulating material with a wide range of applications.[30–32] Considering that graphene and glass show complementary properties in electrical and thermal conductivities, as well as surface wettability, the resultant graphene glass has been shown to be usable in various applications, including low-cost heating devices, transparent electrodes, photocatalytic plates, and biocompatible cell-culture media.[30–33] Various types of solid glass, i.e., quartz glass, borosilicate glass, and sapphire glass, have been used as substrates to grow monolayer and few-layer graphene films using a methane precursor-based atmospheric-pressure CVD (APCVD) method (1000–1100 °C, 1–7 h).[30] The growth of uniform graphene on molten soda-lime-silica glass has also been demonstrated under APCVD conditions (1000 °C, 1–6 h).[31] However, these primitive graphene glass are not suitable for industrial use, owing to the fact that it can currently be produced only in rather small dimensions (less than 4 inches). Further, it exhibits nonuniformity at the macroscopic level and is costly and time consuming (1–7 h) in production.

In this study, we developed an ethanol-precursor-based low-pressure CVD (LPCVD) route for the fast and economical synthesis of highly uniform, large-area, and thickness-controllable graphene glass. The uniqueness of this route lies in the fact that: i) the LPCVD system allows for improvements in the mass-transport rate[17] and concentration uniformity[34] of the active carbon species in the growth zone in contrast to the case for the APCVD route, which results in graphene films with significantly enhanced growth efficiency and thickness uniformity across large areas, and ii) the thermal decomposition rate of ethanol is rather high at temperature greater than 800 °C,[35–37] which ensures the presence of the active carbon species in a sufficient amount for the nucleation and growth of graphene under the low-pressure conditions. As a result, a 25-inch uniform graphene-glass sample was produced within 4 min, the production efficiency of which was ≈20 times faster than that from the methane-precursor-based APCVD method. Marked improvements in the film thickness uniformity, sheet resistance, and transparency were also achieved. Finally, the produced graphene glass was employed as a liquid-crystal-based switchable window and in a biosensor, with both devices showing excellent performances.

Dr. X.-D. Chen, Z. L. Chen, Dr. J. Y. Sun, Dr. H. H. Wang, L. Lin, M. K. Priydarshi, Prof. Y. F. Zhang, Prof. Z. F. Liu
Center for Nanochemistry (CNC)
Beijing Science and Engineering Center for Nanocarbons
Beijing National Laboratory for Molecular Sciences
College of Chemistry and Molecular Engineering
Peking University
Beijing 100871, P. R. China
E-mail: yanfengzhang@pku.edu.cn; zfliu@pku.edu.cn

W.-S. Jiang, W. Xin, Prof. Z.-B. Liu, Prof J.-G. Tian
The Key Laboratory of Weak Light Nonlinear Photonics
Ministry of Education
Teda Applied Physics School and School of Physics
Nankai University
Tianjin 300071, China

Dr. C. H. Zhang, Prof. H. Yang, Prof. Y. F. Zhang
Department of Materials Science and Engineering
College of Engineering
Peking University
Beijing 100871, P. R. China

Prof. Y. Y. Zhang
Department of Chemistry
Tsinghua University
Beijing 100084, China
E-mail: yingyingzhang@tsinghua.edu.cn

DOI: 10.1002/adma.201603428

ADVANCED MATERIALS
www.advmat.de

Materials Views
www.MaterialsViews.com

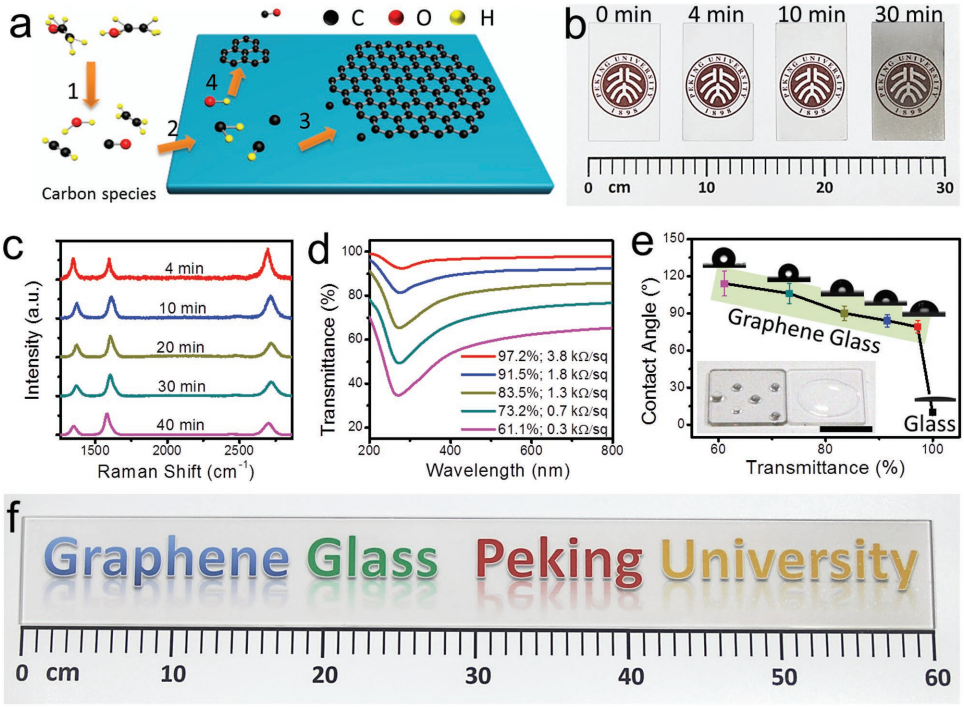

Figure 1. a) Schematic of graphene growth on solid quartz glass by the LPCVD method using ethanol as precursor. Step 1: Thermal decomposition of ethanol, step 2: adsorption and decomposition of carbon species, step 3: diffusion and growth of graphene, and step 4: etching of amorphous carbon. b) Photographs of as-grown graphene-glass samples (10 cm × 6 cm) obtained for growth time of 4, 10, and 30 min; a bare quartz glass (leftmost) is shown for comparison. Growth conditions: Ar/H_2/ethanol: 1000/1000/500 sccm at 1100 °C, 1250 Pa. c–e) Series of Raman spectra (c), transmittance and sheet resistance values (d), and contact angles (e) of graphene-glass samples grown by the ethanol-precursor-based LPCVD route for growth time of 4, 10, 20, 30, and 40 min, respectively. The insets in (e) on the left and right show the hydrophobic and hydrophilic characteristics of the graphene glass and bare glass, respectively. Scale bar: 1 cm. f) Photograph of 25-inch (along diagonal) graphene-glass sample, highlighting its highly uniform film thickness and transmittance.

A schematic of the ethanol-precursor-based LPCVD system is shown in Figure S1 in the Supporting Information. In this system, liquid ethanol is stored in a stainless-steel tank, and the flow rate of the vaporized ethanol is controlled by a mass-flow controller during the CVD process. It is well known that ethanol effectively decomposes into several different carbon species, such as ethylene, acetylene, and $CH_{x\leq4}$, under a relatively high growth temperature (>800 °C).[36,37] As shown in **Figure 1**a, these carbon species first adsorb onto the quartz-glass substrate, then go through the process of nucleating, growing, merging, and eventually forming continuous graphene films in an efficient fashion. Normally, a high concentration of active carbon species is required for the fast growth of graphene, and the mass production of amorphous carbon will greatly degrade the quality of graphene. Specifically, the generation of the amorphous carbons is dramatically suppressed in our case, owing to the etching effect of the OH radicals arising from the decomposition of ethanol.[35,37] For comparison, ethylene, the primary decomposition product of ethanol, was used as precursor to grow graphene glass at the same conditions, where a prominent signal for amorphous carbon was observed in the Raman data shown in Figure S3 in the Supporting Information. The lack of OH radicals in the CVD growth process was considered to lead to the different growth results.

Figure 1b shows photographs of the bare quartz-glass substrate (leftmost, shown as a reference) and the graphene-/quartz-glass samples grown by LPCVD for 4, 10, and 30 min at 1100 °C under the system pressure of 1250 Pa. The thickness of the directly grown graphene films increases (from monolayer to ten layer) by extending the growth time (from left to right), as evidenced by the gradual increase in the gray contrast. This observation is supported by the results of Raman and transmittance measurements (Figure 1c,d). Notably, when the growth time was set to 4 min, the typical Raman signal for monolayer graphene could be observed in the case of the as-grown sample. Moreover, the optical transmittance at 550 nm is found to be 97.2%, with a measured sheet resistance of 3.8 kΩ sq^{-1} (Figure 1d). Further, the C 1s X-ray diffraction (XPS) spectrum of the film contains a dominant sp^2-carbon-related peak (284.5 eV), a C–H-related peak (285.2 eV) and broad C—O-related peaks (Figure S2, Supporting Information). All these results point to the relatively high quality of the as-obtained monolayer graphene grown on glass.

Graphene glass exhibiting excellent optical transparency and good electrical conductivity is essential for it to find wide use. In our study, the transparency and conductivity of the graphene glass with different graphene thickness have been systematically examined. Similar to other conductive films, the two parameters present a negative correlation with the graphene

DOI: 10.1002/adma.201603428

thickness increase (Figure 1d). Representatively, an equilibrium between the transmittance and the electrical conductivity could be achieved at 80% and 1.1 kΩ sq^{-1}, respectively, with the graphene thickness of approximately eight layer. Notably, the two values are superior to those for samples fabricated by APCVD at 76–83% and 1.7–3.5 kΩ sq^{-1},[30] and plasma-enhanced CVD at 77–83% and 2.5–4 kΩ sq^{-1},[38] as well as those of reduced graphene oxide assembled on glass at 79–83% and 8–20 kΩ sq^{-1}, respectively.[39] Herein, the formation of amorphous carbon species was greatly suppressed owing to the small collision probability of the active carbon species under low-pressure conditions[17] and the etching effects of the OH radicals.[35,37] This is the reason why such superior quality of the synthesized graphene glass can be obtained throughout our proposed route.

Along with transparent conducting features, the hydrophobic surface of graphene glass is essential for potential applications such as self-cleaning windows. Figure 1e shows the hydrophobic characteristics of the synthesized samples, as indicated by the plot of the static water contact angle as a function of transmittance. The difference in the wetting characteristics between the pristine and graphene glass is prominent, showing distinct contact angles of ≈10° versus >70°. The contact angle enlarges with increasing the thickness of graphene, reaching 115° for T_{550} value of 61%. This indicates that the direct coating of graphene on glass is key to tailoring the surface hydrophobicity of glass. The inset photograph in Figure 1e shows the distinctive surface wetting behaviors of graphene glass (left) and pristine glass (right).

As mentioned above, the applicability of graphene glass would depend greatly on its reliable and scalable production in large sizes such that it exhibits good uniformity and high performance. In this work, a uniform 25-inch graphene glass (60 mm in width) sample possessing good transparency and uniform graphene coverage were fabricated by means of the ethanol-precursor-based direct LPCVD route (Figure 1f). This is the largest graphene-glass sample produced thus far. It is worthy of mentioning that such graphene-glass samples are difficult to produce by the traditional APCVD growth route using methane as carbon precursor.[30,40]

It is evident that growing graphene on glass or other insulating substrates normally involves lengthy synthesis periods (e.g., 1–7 h) as compared to the use of metal substrates.[23–25,30,40] However, the proposed LPCVD method, using ethanol as the precursor, enables rapid graphene deposition even on glass, completing a full coverage of monolayer graphene on a glass substrate within just 4 min at 1100 °C.

Such rapidly grown graphene samples necessitate a comprehensive characterization of their quality and properties. **Figure 2**a shows a scanning electron microscopy (SEM) image

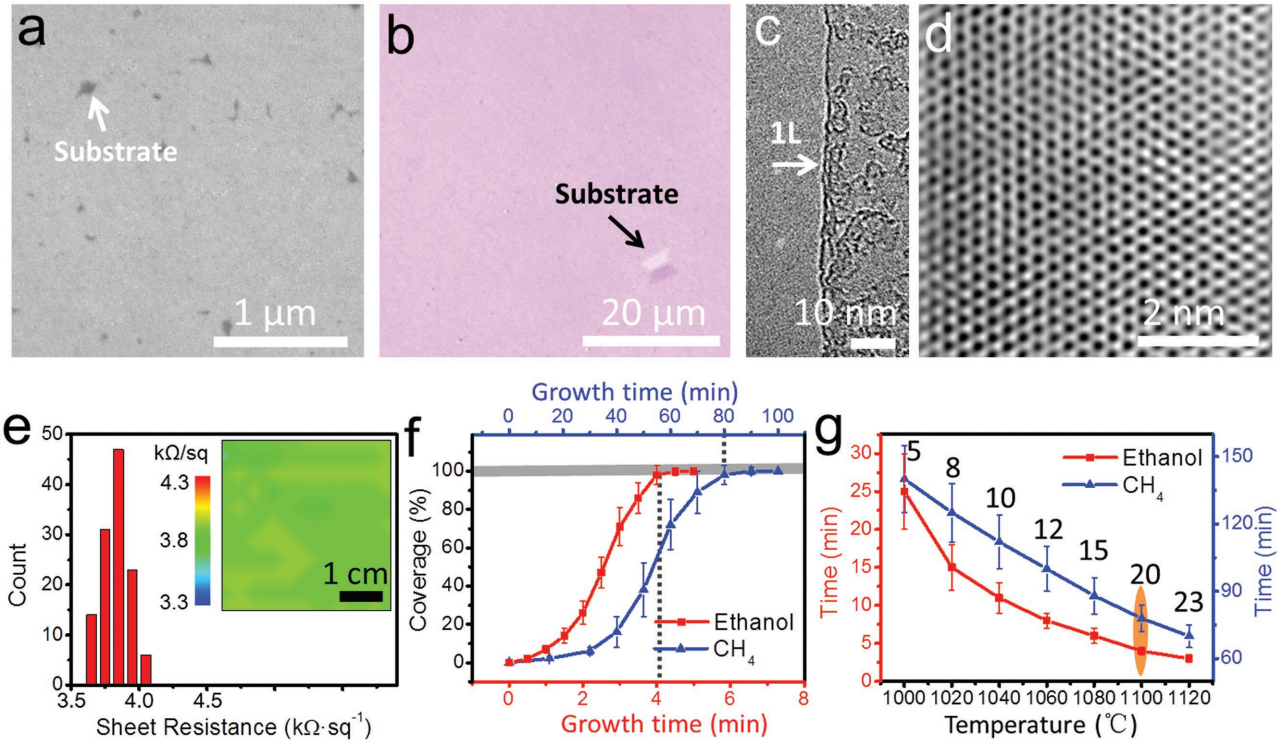

Figure 2. a) SEM image of graphene glass grown by ethanol-precursor-based LPCVD. b) OM image of monolayer graphene (for sample shown in (a)) transferred onto SiO_2/Si. c) HR-TEM image showing uniform monolayer thickness of the graphene film. d) Atomic-resolution TEM image of the monolayer graphene. e) Distribution of sheet resistance (collected from 121 points) of the monolayer graphene glass. Inset shows the spatial distribution of the sheet resistance (5 cm × 5 cm). f) Growth-time dependence of the graphene-glass samples synthesized through the ethanol-precursor-based (red, this work) and methane-precursor-based (blue, previous work) routes. g) Time requirement for growing full-coverage graphene glass via the two synthesis routes at temperatures of 1000–1120 °C. The numbers above the curves (5–23) represent the improvement of the growth efficiency. LPCVD growth conditions: Ar/H_2/ethanol 1000/1000/500 sccm, 1250 Pa; APCVD growth conditions: Ar/H_2/CH_4 500/50/15 sccm.

of the as-synthesized graphene on quartz glass. The different contrasts (light gray and dark gray) represent the graphene area and the bare substrate, respectively. Accordingly, the coverage of graphene has been estimated to be 98%. The uniformity of the film thickness is confirmed by the highly uniform color contrast of the optical microscope (OM) image (Figure 2b), which was acquired after transferring the graphene film onto a SiO_2 substrate. To characterize the structures at the atomic level, the samples were examined using high-resolution transmission electron microscopy (HR-TEM). Sectional views of the film edges show that most samples are of predominantly monolayer thickness (Figure 2c). Further, an atomic-resolved HR-TEM image (Figure 2d) confirms the presence of perfect atomic lattices of graphene.

The large-scale uniformity and stability of the monolayer graphene films grown on glass were also evaluated by mapping their sheet resistances using a macroscopic four-probe technique (5 cm × 5 cm). The distribution of the sheet resistance data (collected from 121 points) is plotted in Figure 2e, showing an average value of ≈3.8 kΩ sq^{-1}. The corresponding mapping graph displays uniform green color in most regions (Figure 2e inset), further confirming the excellent film uniformity and conductivity of the graphene glass produced by the ethanol-precursor-based LPCVD route. In addition, stability measurements of the sheet resistance indicate that the resistance values remain unchanged even after storing the samples in air at room temperature for 30 d (Figure S4, Supporting Information).

For the direct growth of graphene on insulators, APCVD-based methods have been mainly employed with methane as the typical carbon precurser.[23,24,30,31] In contrast, synthesis by the LPCVD route depends strongly on the carbon precursor used. An appropriate precursor can improve growth efficiency and graphene uniformity concurrently. It is known that, under low-pressure conditions, the rate determining step for the CVD growth of graphene is the surface reactions, given the rather high mass-transport rate.[17] This is actually attributed to the high diffusivity of the active carbon species in the low-density environment.[17,34] In contrast, under atmospheric-pressure conditions, the mass-transport rate is limited, since the transport coefficient is several orders of magnitude smaller than that under low-pressure conditions.[17,34] Hence, the LPCVD route is, in general, more suitable for the fast deposition of graphene.

To explore the growth dynamics as well as the fast-growth behavior, growth results obtained through the ethanel-precurser-based LPCVD route and the traditional methane-precursor-based APCVD route were systematically compared. Specifically, the coverage of submonolayer graphene as a function of the growth time (for growth at 1100 °C) is plotted in Figure 2f. When ethanol is used as a precursor, nucleation occurs very quickly (in 30 s), and then the coverage increases rapidly with the increase of the growth time, where full-coverage monolayer graphene could be grown on glass within 4 min. In contrast, the growth efficiency is much lower when methane is used as the precursor: at the nucleation stage, nuclei are not observed until a synthesis time of 30 min; furthermore, it is difficult to obtain full-coverage graphene films on glass even after 80 min. In this regard, it is worth noting that the growth efficiency corresponding to the ethanol-precursor-based LPCVD route is ≈20 times higher than that for the methane-precursor-based APCVD route.[17,34]

The system pressure is found to be a key factor to the growth of graphene on glass. As discussed in Discussion S1 in the Supporting Information, lower pressure will lead to less gas collisions and higher mass transport coefficient, while the concentration of carbon species is also greatly decreased. Glass is catalytically inert with respect to the decomposition of carbon precursors, and a rather high concentration of the carbon species is required for the growth of graphene on glass than that on metal substrates.[30,31] In fact, the graphene is hardly grown on glass using methane as precursor under a LPCVD route (Figure S5a, Supporting Information), owing to the relative low thermal-decomposition efficiency and the small concentration of methane under low-pressure conditions. In contrast, ethanol can be efficiently decomposed at temperatures >800 °C,[36,37] and sufficient active carbon species can thus be provided for the nucleation and the growth of graphene on glass via the LPCVD route. However, when the system pressure is smaller than the optimum pressure (1250 Pa in our experiments), the concentration of carbon species will be lowered, leading to decreased growth rate of graphene on glass (Figure S5b, Supporting Information).

The growth efficiency can be further augmented by increasing the ethanol feeding rate. However, doing so could lead to a decrease in the domain sizes and an increase in the defect density, greatly degrading the quality of graphene (Figure S6, Supporting Information). The detailed flow rates of the ethanol vapor and methane used for the growth of full-coverage graphene glass with different growth time are compared in Table S1 in the Supporting Information and discussed in Discussion S1 in the Supporting Information. For the typical fast growth of monolayer graphene glass (growth time of 4 min), the ratio of the Raman D peak intensity to the G peak intensity (I_D/I_G) was ≈1, which compares favorably with that from previously reported graphene glass grown by methane-precursor-based APCVD (I_D/I_G ≈ 0.8–1.2).[30,40]

To investigate the effect of the growth temperature, temperature-dependent syntheses (1000–1120 °C) of monolayer graphene on quartz glass were performed via the two different growth routes (Figure 2g). Intriguingly, the growth time in the case of the proposed LPCVD route using ethanol as the precursor could be remarkably reduced, from 25 to 3 min, by varying the temperature from 1000 to 1120 °C. This renders our process 5–23 times faster than the traditional APCVD method employing methane as the precursor. Further, great improvement of the surface-deposition rate can be achieved by the LPCVD route as compared to the APCVD route when the growth temperature increases (Section S1, Supporting Information).[34] Consequently, our proposed route has a clear advantage over the APCVD route for synthesis at elevated temperature.

To highlight the macroscopic uniformity of the synthesized large-scale graphene-glass samples, digital photographs of the 25-inch graphene-glass samples as well as their schematic views are shown in **Figure 3**a,b, respectively. For comparison, two pieces of graphene glass were respectively synthesized using ethanol and methane as the precursor. The marked difference in the color contrasts in the photographs indicates that the graphene-glass sample grown using ethanol possesses excellent thickness uniformity, whilst the sample grown using methane exhibits a gradual increase in film thickness along

Adv. Mater. **2016**,
DOI: 10.1002/adma.201603428

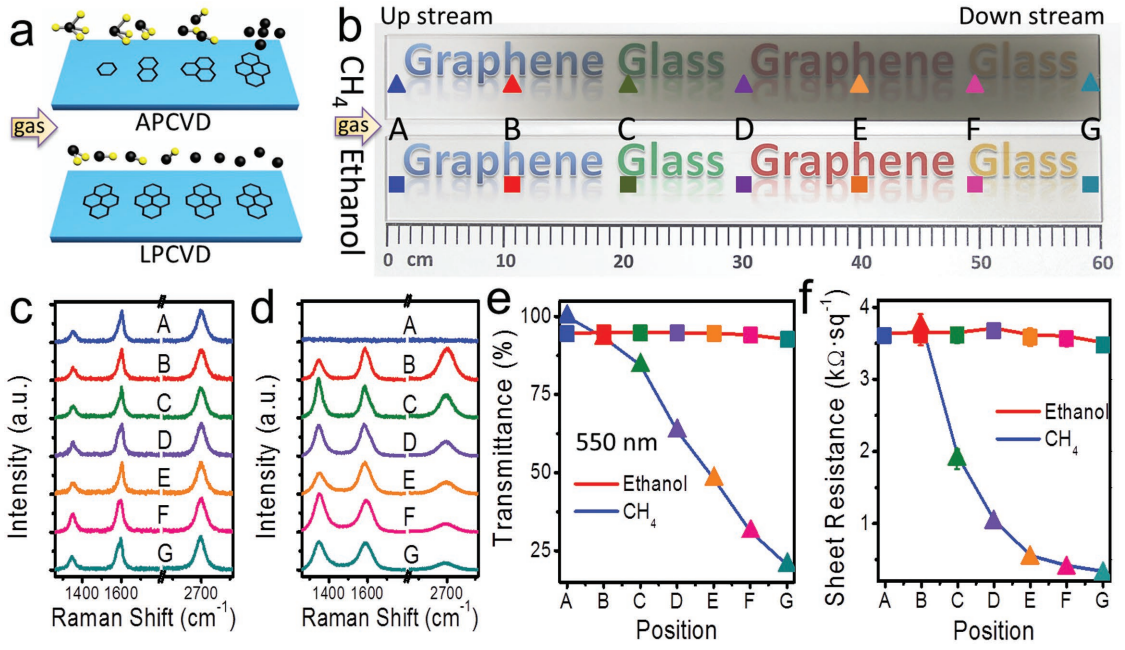

Figure 3. a) Schematic views showing distributions of active carbon species on growth substrates under APCVD and LPCVD conditions, respectively. b) Photograph of 25-inch graphene-glass samples grown by methane-precursor-based APCVD (up) and ethanol-precursor-based LPCVD (down) methods. The gas flow direction was from left to right. c,d) Raman spectra of the graphene-glass samples synthesized using ethanol (c) and methane (d) collected from positions labeled A–G in (b). The former sample shows greater thickness uniformity than that of the latter one over a nearly macroscopic distance of ≈60 cm. e,f) Differences in the transmittance (e) and sheet resistance (f) values of the graphene samples synthesized using methane (triangles) and ethanol (squares) precursors (measured at locations A–G in (b)). Obviously, the sample obtained by the ethanol-precursor-based LPCVD synthesis route exhibits uniform transmittance and sheet resistance.

the gas flow direction (Figure 3b). This phenomenon can be explained based on the concentration distribution of the active carbon species in the reaction chamber. During the APCVD process (Figure 3a), the concentration of the active carbon species is significantly increasing along the gas flow direction in the heating zone.[34] This results in the graphene films at the downstream positions being thicker than those at the upstream positions. However,, the situation in the LPCVD system is much different, since the active carbon species are distributed uniformly in the chamber, resulting in relatively stable growth efficiency in the growth zone. As a result, large-area uniform graphene glass can be grown with ease.

To further highlight the remarkable difference in the film uniformity produced using the two different methods, survey Raman measurements were performed at selected points (marked in Figure 3b with rectangles and triangles) on the graphene-glass samples produced using ethanol and methane as precursors (Figure 3c,d). All the Raman spectra in Figure 3c contain small D band peaks and sharp 2D band peaks, which are indicative of good film uniformity and sample quality over the lateral distance of 60 cm. However, the shapes of the Raman spectra of the graphene glass grown using methane are highly inconsistent and vary significantly from point to point. The thickness of this graphene film increases dramatically along the gas flow direction. Moreover, strong amorphous carbon-related signals can be observed at the downstream points (e.g., positions E, F, and G in Figure 3d). The transmittance and sheet resistance measurement results, shown in Figure 3e,f, further confirm the rather high uniformity of the LPCVD-based graphene-glass sample, corroborating the data obtained from the Raman measurements.

A key advantage of the proposed method is to allow for the fast and low-cost production of 25-inch-scale, highly uniform graphene-glass samples. This should promote the practical use of such glass that is difficult to achieve otherwise. To demonstrate this, a large-area switchable window was fabricated using the synthesized graphene glass. A layer of polymer-dispersed liquid crystal (PDLC, 20 μm thick) is sandwiched between two pieces of graphene glass with transmittance of 90%, as shown schematically in **Figure 4**a. The alignment of the liquid crystal molecules, and thus the transparency of the window, could be controlled by applying a suitable electric field.[41] Figure 4b shows a photograph of a typical 25-inch switchable window constructed using the graphene glass grown by ethanol-precursor-based LPCVD. The window could be switched immediately from the scattering state (opaque and ivory white) to the transparent state by applying a voltage of 35 V, a safe value for human contact. For comparison, an indium tin oxide (ITO, 90% transmittance)/glass-based switchable window with the same configuration was also constructed.

Figure 4c shows the bias-voltage-induced variations in the transmittances of the two devices. Both threshold voltage (V_{th}) and saturation voltage (V_{sat}) of the graphene-glass-based device are smaller than those of the ITO/glass-based one, owing to the possible interaction between graphene and liquid crystal.[42] Thus a relatively small voltage is required to drive such a

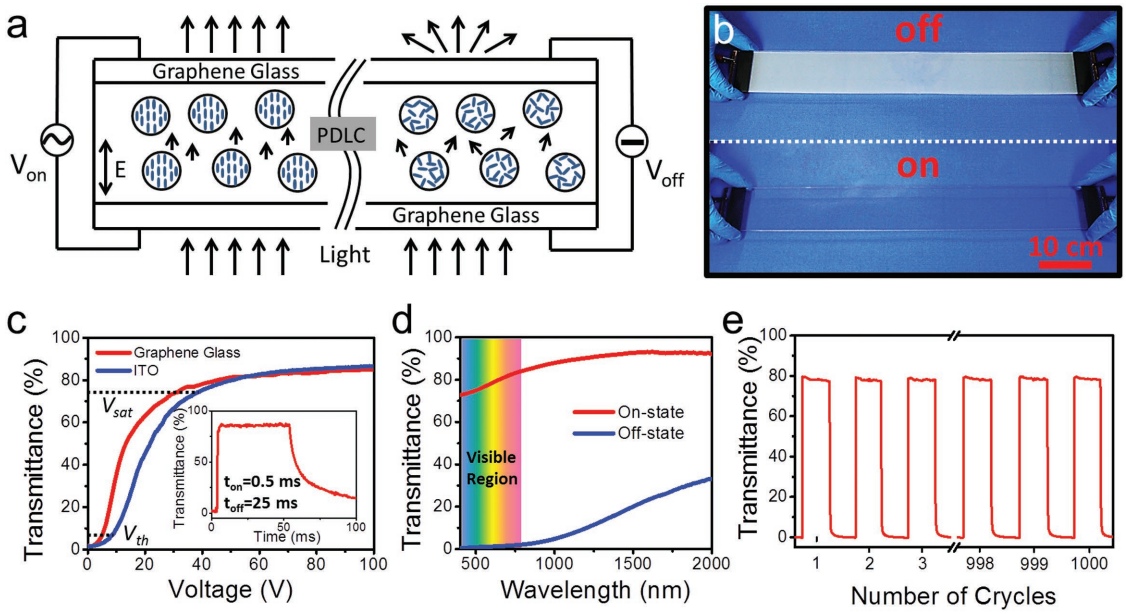

Figure 4. a) Schematic of the graphene-glass-based switchable window with power on (left) and off (right). b) Photographs of the 25-inch graphene-glass-based switchable window in the off state (up) and on state (down) for a voltage of 35 V. c) Comparison of the transmittances of the graphene-glass-based and ITO/glass-based switchable windows as a function of the applied voltage. Inset shows the response time of the graphene-glass-based switchable window. d) Transmittances in the off-state and on-state of the graphene-glass-based switchable window. e) Results of the cycling test of the switchable window under a periodic voltage, highlighting its robustness.

graphene-glass-based switchable window. Moreover, the graphene-glass-based switchable window exhibits quite short rise (≈0.5 ms) and decay time (≈25 ms) (inset of Figure 4c), and the contrast ratio (T_{on}/T_{off}) of the switchable window based on graphene glass is higher than 120 at the visible region (Figure 4d), suggesting the high performance of the device. In order to make it an actually usable device in daily life, the robustness was rigorously tested. Apparently, the response time and contrast ratio of the device remain constant during the entire test process (i.e., for 1000 cycles) (Figure 4e). It can therefore be concluded that graphene glass can serve as a perfect alternative to ITO/glass in liquid-crystal-based switchable windows, owing to its good transparency, small drive voltage, rapid response, large contrast ratio and high durability.

In addition, the graphene glass synthesized in this study showed great potential for use in biosensors, offering an attractive alternative to conventional biosensors based on surface plasmon resonance (SPR) for the real-time detection and monitoring of biomolecular interactions.[43,44] As shown in **Figure 5**a, a graphene-glass-based biosensor with multiple functional layers encompassing (poly(dimethylsiloxane) (PDMS) microfluidic channel/graphene/glass/prism) has been constructed. The principle of detection is based on the polarization-dependent optical absorption property of graphene under total internal reflection (TIR) (Discussion S2, Supporting Information).[45,46] A biorecognition element (antigen) is bound onto the graphene surface to detect a specific biomolecule (antibody) in solution (Figure 5b), while a polarized laser has been used to detect the resulting signal (Figure S8, Supporting Information).

The results of the real-time detection of a 100 μg mL^{-1} anti-IgG (protein, antibody) solution using the graphene-glass-based biosensor are shown in Figure 5c and Figure S9 (Supporting Information). Owing to the specific binding of the antigen and antibody on the graphene surface, the optical absorption of graphene under TIR is enhanced, with the output being measured in the form of a voltage difference (1.25 V for 100 μg mL^{-1} anti-IgG solution) by a balanced detector. The anti-IgG is dissociated from the IgG on graphene surface by injecting phosphate buffer saline (PBS) and glycine, resulting in a large voltage drop. Thus the biosenor can be operated repeatedly, and presents repeatable signals (Figure S9, Supporting Information). The ability of the biosensor to detect anti-IgG solutions of lower concentrations (10 and 0.10 μg mL^{-1}, Figure S10, Supporting Information) has also been tested in order to determine the detection limit of the biosensor. Under optimized conditions, the biosensor based on graphene glass achieves a detection limit of 0.10 μg mL^{-1} and exhibits a satisfactory response to anti-IgG for concentrations of 0.10–100.00 μg mL^{-1} (Figure 5d). This response is superior to that of Au-film-based SPR biosensors (2.50–20.00 μg mL^{-1}) and comparable to that of Au-nanoparticle-based SPR biosensors (0.30–20.00 μg mL^{-1}).[47] The specificity of the device has also been tested by injecting 100 μg mL^{-1} bovine serum albumin (BSA, nonspecific antibody) solution and 100 μg mL^{-1} anti-IgG solution, respectively. The response from the mismatched BSA is significantly smaller than that from the complementary anti-IgG (Figure S11, Supporting Information), indicating the excellent specificity of the biosensor. Finally, for comparison, anti-IgG solutions with concentrations of 0.625–5 μg mL^{-1} are detected using a commercial SPR biosensor (Figure S12, Supporting Information), for which the detection of 0.625 μg mL^{-1} is difficult to achieve. Therefore, the graphene-glass-based biosensor has great

Adv. Mater. **2016**,
DOI: 10.1002/adma.201603428

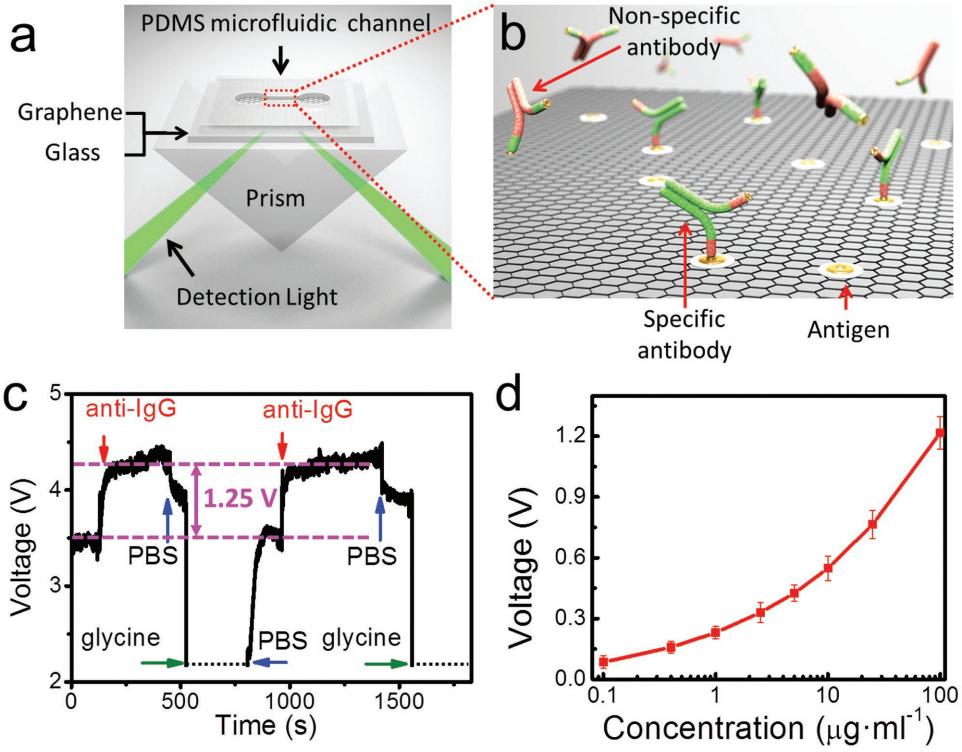

Figure 5. a) Structure of the graphene-glass-based biosensor. b) Process of specific binding of the antigen (protein) and antibody (protein). c) Real-time response of the graphene-glass-based biosensor to 100 μg mL^{-1} anti-IgG solution. Red, blue, and green arrows represent the injection of anti-IgG, PBS, and glycine, respectively. Subsequently, the detection cycle again started from the beginning. d) Detection limit of the graphene-glass-based biosensor, showing that it could detect a solution with a concentration of 0.10 μg mL^{-1} with a satisfactory response of 0.09 V.

potential for use in various practical applications, owing to its various advantages, such as high performance, low cost, and ease of fabrication.

To sum up, we have developed an ethanol-precursor-based LPCVD route for the fast growth of 25-inch-long uniform graphene-glass samples in a very short period of time (growth time of 4 min). Our proposed route showed much improved synthesis efficiency (10–20 times faster) as compared to that of the prevalent methane-precursor-based APCVD route. Moreover, such a synthetic strategy guaranteed large-scale production of graphene films with significantly improved uniformity in thickness, transmittance, and sheet resistance. The large-area, highly uniform graphene glass synthesized using the proposed method already found wide use in numerous practical applications, e.g., in liquid-crystal-based switchable windows and in biosensors. In essence, this work provides a reliable pathway for the scalable production of high-quality graphene glass, further offering novel insights into the usage of such unique graphene-glass hybrid materials in next-generation applications at an industrial level.

Experimental Section

Ethanol Precursor-Based LPCVD Growth of Graphene Glass: In a typical CVD process, thoroughly cleaned quartz glass was loaded into a horizontal quartz tube (3-inch diameter) inside of a three-zone high-temperature furnace (Lindberg/Blue). The quartz tube was pumped to ≈1 Pa to clean the system, and then filled with 200 sccm Ar and 200 sccm H_2 followed by heating the furnace to the desired growth temperature (1000–1120 °C). When the tube reached the desired temperature and stabilized for 10 min, the Ar/H_2 flow rate were changed to 1000/1000 sccm, and 500 sccm ethanol vapor was then pumped into the chamber for a certain time. The partial pressure of ethanol was 250 Pa. After the growth, ethanol was cut off, and the sample was fast cooled down by sliding the sample out of the furnace.

Methane Precursor-Based APCVD Growth of Graphene Glass: The same quartz tube and furnace were used in experiments. Prior to heating, the chamber was flushed with 500 sccm Ar to remove air. Typical growth conditions were 500 sccm Ar, 50 sccm H_2, and 15 sccm CH_4 at 1000–1120 °C for 1–3 h.

Graphene-Glass-Based Switchable Window: The graphene-glass-based switchable window consists of two pieces of graphene glass and a sandwiched PDLC layer. In this work, 68.5% nematic liquid crystal (SLC-1717, T_{NI} = 365.2 K, n_o = 1.519, n_e = 1.720), 30% comonomers (stearyl acrylate/3,5,5-trimethelhexyl acrylate/1,4-butanedioldiacrylate 2/2/1), and 1.5% initiator (2,2-dimethoxy-1,2-diphenyl-ethanone) were mixed homogeneously and then were injected into the gap (20 μm) between two graphene glass. The mixture was exposed to a 35 W Hg lamp for 7 min to polymerize the PDLC layer. The performance of the switchable window was measured using the liquid-crystal device parameters tester (LCT-5016C).

Graphene-Glass-Based Biosensor: The graphene-glass-based biosensor consists of PDMS-microfluidic-channel/graphene/glass/prism. The thickness of the graphene film is ≈8 nm, which is the optimum thickness for the detection. Firstly, the microfluidic channel and graphene glass was packaged by oxygen plasma treatment and then attached to a K9 glass prism with index matching fluid. Then the rabbit IgG (antigen) solution

(1 mg mL^{-1}) was slowly injected into the microfluidic channel using a syringe pump and was heated at 35 °C for 1 h to achieve better binding onto graphene surface. The redundant antigen was rinsed by PBS. Circularly polarized light (532 nm) was focused by a 50× objective lens, and entered the prism with normal incidence. The light was totally reflected at the glass/graphene/liquid interface and separated into transverse electric (TE) and transverse magnetic (TM) modes by a polarization beam splitter. The power difference of the TE- and TM-polarized light was detected by a balanced photodetector (THORLABS PDB210A). The commercial SPR sensor used was Biacore X100(GE).

Characterization: The prepared samples were systematically characterized using optical microscopy (Olympus DX51), SEM (Hitachi S-4800, operating at 1 kV), Raman spectroscopy (Horiba, LabRAM HR-800, 514 nm laser excitation, 100 × objective lens), UV–vis spectroscopy (Perkin–Elmer Lambda 950 spectrophotometer), XPS (Kratos Analytical Axis-Ultra spectrometer using a monochromatic Al K_α X-ray source), contact angle system (DataPhysics, OCA20), TEM (FET Tecnai F20, 200 kV; JEM-ARM200F equipped with double postspecimen spherical aberration correctors, 80 kV), and four-probe resistance measuring meter (Guangzhou 4-probe Tech Co. Ltd., RTS-4).

Supporting Information

Supporting Information is available from the Wiley Online Library or from the author.

Acknowledgements

This work was financially supported by the Ministry of Science and Technology of China (2016YFA0200103 and 2013CB932603), the National Natural Science Foundation of China (51432002, 51290272, and 51472008), the Beijing Municipal Science and Technology Planning Project (Z151100003315013), and the Certificate of China Postdoctoral Science Foundation Grant (2016M590010).

Received: June 29, 2016
Revised: September 3, 2016
Published online:

[1] K. S. Novoselov, A. K. Geim, S. V. Morozov, D. Jiang, Y. Zhang, S. V. Dubonos, I. V. Grigorieva, A. A. Firsov, *Science* **2004**, *306*, 666.
[2] K. S. Novoselov, A. K. Geim, S. V. Morozov, D. Jiang, M. I. Katsnelson, I. V. Grigorieva, S. V. Dubonos, A. A. Firsov, *Nature* **2005**, *438*, 197.
[3] A. S. Mayorov, R. V. Gorbachev, S. V. Morozov, L. Britnell, R. Jalil, L. A. Ponomarenko, P. Blake, K. S. Novoselov, K. Watanabe, T. Taniguchi, A. K. Geim, *Nano Lett.* **2011**, *11*, 2396.
[4] C. Lee, X. Wei, J. W. Kysar, J. Hone, *Science* **2008**, *321*, 385.
[5] A. A. Balandin, *Nat. Mater.* **2011**, *10*, 569.
[6] R. R. Nair, P. Blake, A. N. Grigorenko, K. S. Novoselov, T. J. Booth, T. Stauber, N. M. R. Peres, A. K. Geim, *Science* **2008**, *320*, 1308.
[7] H. Zhang, X. Lv, Y. Li, Y. Wang, J. Li, *ACS Nano* **2010**, *4*, 380.
[8] S. Bae, H. Kim, Y. Lee, X. Xu, J.-S. Park, Y. Zheng, J. Balakrishnan, T. Lei, H. R. Kim, Y. I. Song, Y.-J. Kim, K. S. Kim, B. Ozyilmaz, J.-H. Ahn, B. H. Hong, S. Iijima, *Nat. Nanotech.* **2010**, *5*, 574.
[9] Q. Wu, Y. Xu, Z. Yao, A. Liu, G. Shi, *ACS Nano* **2010**, *4*, 1963.
[10] F. Xia, T. Mueller, Y.-m. Lin, A. Valdes-Garcia, P. Avouris, *Nat. Nanotechnol.* **2009**, *4*, 839.
[11] N. M. Gabor, J. C. W. Song, Q. Ma, N. L. Nair, T. Taychatanapat, K. Watanabe, T. Taniguchi, L. S. Levitov, P. Jarillo-Herrero, *Science* **2011**, *334*, 648.
[12] Y. Hernandez, V. Nicolosi, M. Lotya, F. M. Blighe, Z. Sun, S. De, I. T. McGovern, B. Holland, M. Byrne, Y. K. Gun'ko, J. J. Boland, P. Niraj, G. Duesberg, S. Krishnamurthy, R. Goodhue, J. Hutchison, V. Scardaci, A. C. Ferrari, J. N. Coleman, *Nat. Nanotechnol.* **2008**, *3*, 563.
[13] G. Eda, G. Fanchini, M. Chhowalla, *Nat. Nanotechnol.* **2008**, *3*, 270.
[14] X. Li, W. Cai, J. An, S. Kim, J. Nah, D. Yang, R. Piner, A. Velamakanni, I. Jung, E. Tutuc, S. K. Banerjee, L. Colombo, R. S. Ruoff, *Science* **2009**, *324*, 1312.
[15] A. Reina, X. Jia, J. Ho, D. Nezich, H. Son, V. Bulovic, M. S. Dresselhaus, J. Kong, *Nano Lett.* **2009**, *9*, 30.
[16] Y. Hao, M. S. Bharathi, L. Wang, Y. Liu, H. Chen, S. Nie, X. Wang, H. Chou, C. Tan, B. Fallahazad, H. Ramanarayan, C. W. Magnuson, E. Tutuc, B. I. Yakobson, K. F. McCarty, Y.-W. Zhang, P. Kim, J. Hone, L. Colombo, R. S. Ruoff, *Science* **2013**, *342*, 720.
[17] S. Bhaviripudi, X. Jia, M. S. Dresselhaus, J. Kong, *Nano Lett.* **2010**, *10*, 4128.
[18] T. Wu, X. Zhang, Q. Yuan, J. Xue, G. Lu, Z. Liu, H. Wang, H. Wang, F. Ding, Q. Yu, X. Xie, M. Jiang, *Nat. Mater.* **2016**, *15*, 43.
[19] H. Zhou, W. J. Yu, L. Liu, R. Cheng, Y. Chen, X. Huang, Y. Liu, Y. Wang, Y. Huang, X. Duan, *Nat. Commun.* **2013**, *4*, 2096.
[20] X. Li, Y. Zhu, W. Cai, M. Borysiak, B. Han, D. Chen, R. D. Piner, L. Colombo, R. S. Ruoff, *Nano Lett.* **2009**, *9*, 4359.
[21] L. Gao, W. Ren, H. Xu, L. Jin, Z. Wang, T. Ma, L.-P. Ma, Z. Zhang, Q. Fu, L.-M. Peng, X. Bao, H.-M. Cheng, *Nat. Commun.* **2012**, *3*, 699.
[22] X. Liang, B. A. Sperling, I. Calizo, G. Cheng, C. A. Hacker, Q. Zhang, Y. Obeng, K. Yan, H. Peng, Q. Li, X. Zhu, H. Yuan, A. R. H. Walker, Z. Liu, L.-m. Peng, C. A. Richter, *ACS Nano* **2011**, *5*, 9144.
[23] J. Chen, Y. Wen, Y. Guo, B. Wu, L. Huang, Y. Xue, D. Geng, D. Wang, G. Yu, Y. Liu, *J. Am. Chem. Soc.* **2011**, *133*, 17548.
[24] J. Chen, Y. Guo, L. Jiang, Z. Xu, L. Huang, Y. Xue, D. Geng, B. Wu, W. Hu, G. Yu, Y. Liu, *Adv. Mater.* **2014**, *26*, 1348.
[25] J. Chen, Y. Guo, Y. Wen, L. Huang, Y. Xue, D. Geng, B. Wu, B. Luo, G. Yu, Y. Liu, *Adv. Mater.* **2013**, *25*, 992.
[26] D. Wei, Y. Lu, C. Han, T. Niu, W. Chen, A. T. S. Wee, *Angew. Chem., Int. Ed.* **2013**, *52*, 14121.
[27] L. Wang, B. Wu, J. Chen, H. Liu, P. Hu, Y. Liu, *Adv. Mater.* **2014**, *26*, 1559.
[28] T. Gao, X. Song, H. Du, Y. Nie, Y. Chen, Q. Ji, J. Sun, Y. Yang, Y. Zhang, Z. Liu, *Nat. Commun.* **2015**, *6*, 6835.
[29] L. Gao, G.-X. Ni, Y. Liu, B. Liu, A. H. Castro Neto, K. P. Loh, *Nature* **2014**, *505*, 190.
[30] J. Sun, Y. Chen, M. K. Priydarshi, Z. Chen, A. Bachmatiuk, Z. Zou, Z. Chen, X. Song, Y. Gao, M. H. Ruemmeli, Y. Zhang, Z. Liu, *Nano Lett.* **2015**, *15*, 5846.
[31] Y. Chen, J. Sun, J. Gao, F. Du, Q. Han, Y. Nie, Z. Chen, A. Bachmatiuk, M. K. Priydarshi, D. Ma, X. Song, X. Wu, C. Xiong, M. H. Rümmeli, F. Ding, Y. Zhang, Z. Liu, *Adv. Mater.* **2015**, *27*, 7839.
[32] J. Sun, Y. Chen, X. Cai, B. Ma, Z. Chen, M. K. Priydarshi, K. Chen, T. Gao, X. Song, Q. Ji, X. Guo, D. Zou, Y. Zhang, Z. Liu, *Nano Res.* **2015**, *8*, 3496.
[33] X.-D. Chen, Z. Chen, J. Sun, Y. Zhang, Z. Liu, *Acta Phys. Chim. Sin.* **2016**, *32*, 14.
[34] G. Li, S.-H. Huang, Z. Li, *Phys. Chem. Chem. Phys.* **2015**, *17*, 22832.
[35] S. Maruyama, R. Kojima, Y. Miyauchi, S. Chiashi, M. Kohno, *Chem. Phys. Lett.* **2002**, *360*, 229.
[36] R. Xiang, B. Hou, E. Einarsson, P. Zhao, S. Harish, K. Morimoto, Y. Miyauchi, S. Chiashi, Z. Tang, S. Maruyama, *ACS Nano* **2013**, *7*, 3095.
[37] B. Hou, R. Xiang, T. Inoue, E. Einarsson, S. Chiashi, J. Shiomi, A. Miyoshi, S. Maruyama, *Jpn. J. Appl. Phys.* **2011**, *50*, 065101.
[38] H. Medina, Y.-C. Lin, C. Jin, C.-C. Lu, C.-H. Yeh, K.-P. Huang, K. Suenaga, J. Robertson, P.-W. Chiu, *Adv. Funct. Mater.* **2012**, *22*, 2123.

[39] X. Li, G. Zhang, X. Bai, X. Sun, X. Wang, E. Wang, H. Dai, *Nat. Nanotech.* **2008**, *3*, 538.
[40] L. Tan, M. Zeng, Q. Wu, L. Chen, J. Wang, T. Zhang, J. Eckert, M. H. Ruemmeli, L. Fu, *Small* **2015**, *11*, 1840.
[41] F. Liu, H. Cao, Q. Mao, P. Song, H. Yang, *Liq. Cryst.* **2012**, *39*, 419.
[42] D. W. Kim, Y. H. Kim, H. S. Jeong, H.-T. Jung, *Nat. Nanotechnol.* **2012**, *7*, 29.
[43] J. Homola, *Chem. Rev.* **2008**, *108*, 462.
[44] T. R. J. Holford, F. Davis, S. P. J. Higson, *Biosens. Bioelectron.* **2012**, *34*, 12.
[45] Q. Ye, J. Wang, Z. Liu, Z.-C. Deng, X.-T. Kong, F. Xing, X.-D. Chen, W.-Y. Zhou, C.-P. Zhang, J.-G. Tian, *Appl. Phys. Lett.* **2013**, *102*.
[46] F. Xing, G.-X. Meng, Q. Zhang, L.-T. Pan, P. Wang, Z.-B. Liu, W.-S. Jiang, Y. Chen, J.-G. Tian, *Nano Lett.* **2014**, *14*, 3563.
[47] L. Wang, Y. Sun, J. Wang, J. Wang, A. Yu, H. Zhang, D. Song, *J. Colloid Interface Sci.* **2010**, *351*, 392.